C. R. Physique 12 (2011) 888–897

Contents lists available at SciVerse ScienceDirect

Comptes Rendus Physique

www.sciencedirect.com

Nano- and micro-optomechanical systems / Nano- et micro-résonateurs optomécaniques

Optomechanical issues in the gravitational wave detector Advanced VIRGO

Phénomènes opto-mécaniques dans le détecteur d'ondes gravitationnelles Advanced VIRGO

Walid Chaibi [a,*], François Bondu [b]

[a] *Département ARTEMIS, Observatoire de la Côte d'Azûr, CNRS, université de Nice Sophia Antipolis, boulevard de l'Observatoire, 06304 Nice cedex, France*
[b] *Institut de physique de Rennes, CNRS, université de Rennes 1, 35042 Rennes, France*

ARTICLE INFO

Article history:
Received 7 July 2011
Accepted 26 July 2011
Available online 13 November 2011

Keywords:
Gravitational waves
Optical cavities
Optical spring
Radiation pressure noise

Mots-clés :
Ondes gravitationnelles
Cavités optiques
Ressort optique
Bruit de la pression de radiation

ABSTRACT

The next generation of the gravitational wave detector VIRGO, namely Advanced VIRGO, will feel an enhancement of optomechanical effects. In fact, it is planned that cavities will be antisymmetrically detuned to compensate symmetry defects between the two arms, which then allows DC detection. In this article, we show that even with slight detuning, the high intra-cavity power stored within the Fabry–Perot cavities makes optical spring effects important enough to constrain the detector adjustment procedure and to limit its sensitivity.

RÉSUMÉ

Dans l'interféromètre, Advanced VIRGO, seconde génération de l'antenne gravitationnelle VIRGO, les effets opto-mécaniques seront d'une importance capitale pour le fonctionnement global du système. En effet, afin de compenser les défauts de symétrie entre les deux bras du Michelson, les cavités optiques devront être désaccordés de manière dissymétrique. Ceci permettra de mettre en place un schéma de détection DC. Dans cet article, on démontre que même dans le cas d'un faible désaccord, la puissance laser intra-cavité rend les effets de ressorts optiques suffisamment importants pour contraindre le contrôle de l'interféromètre et limiter sa sensibilité.

1. Introduction

Currently, an international array of first generation, kilometre-scale laser interferometric gravitational wave detectors, consisting of VIRGO, LIGO, TAMA 300 and GEO600, targeted at gravitational waves in the acoustic band from 10 Hz to 10 kHz, is in operation.

The basic configuration is a Michelson interferometer with Fabry–Perot cavities (Fig. 1) made of two suspended mirrors in each arm and employing power recycling [1]. When subjected to (+) polarisation gravitational radiation, opposite length changes are induced in each arm. Phase changes on the optical field are then read out at the detection port. The Fabry–Perot

* Corresponding author.
E-mail address: chaibi@oca.eu (W. Chaibi).

1631-0705/$ – see front matter
doi:10.1016/j.crhy.2011.07.004

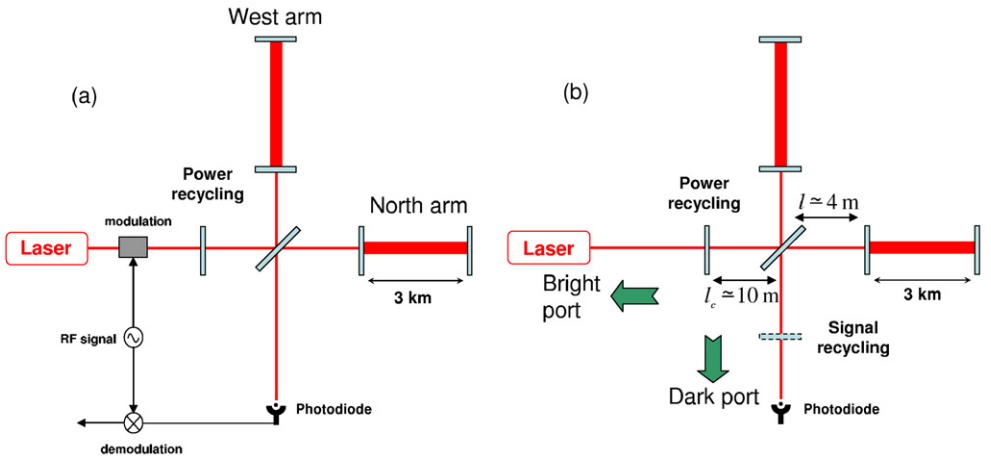

Fig. 1. Schema of VIRGO. The signal is collected on the dark port: (a) Heterodyne schema detection. (b) DC read-out detection, signal recycling will not be treated.

cavities increase the storage time of the light, the phase of which is therefore more sensitive to cavity length variations. In the present status of interferometric gravitational wave (GW) detectors, the main limitation to sensitivity is the thermal noise of the suspension and mirrors for frequencies lower than 200 Hz. At higher frequencies the performance is limited by the shot noise of light, which leads to an error in the measurement of the interferometer output phase [2].

The next step shall be to increase the GW detectors sensitivity up to the quantum limits of the detector [3,4]. The high frequency sensitivity is expected to be improved through shot-noise reduction, achieved by increasing the power circulating in the Fabry–Perot cavities of the detector. However, this procedure promotes the quantum radiation pressure noise in the interferometer to a dominant role at low frequency [5].

In the current generation interferometric gravitational wave detector VIRGO [6], the 3 kilometre-long cavities are at resonance, and the phase variation measurement involves heterodyne detection. However, in the next generation of detectors, the design involves DC detection [7], and a slight detuning of the cavities is introduced, the amplitude of which depends on the symmetry defects between the two arms (mainly 50 ppm loss difference between the two cavities). We expect an improvement of the shot-noise-limited resolution, since there will be no contribution from the phase-modulated sideband noise.

The aim of this article is to discuss some optomechanical issues in the gravitational wave detector Advanced VIRGO. However, recycling signal effects will not be treated, and we send the reader to Refs. [8–10]. In the second section, a calculation framework based on Ref. [11] and describing the coupling between the electromagnetic wave and the mirrors motion in the frequency domain is introduced. In detuned Fabry–Perot cavities, optical spring effects are enhanced, and will then be presented in the third section. Then, in the fourth section, mirrors control issues will be discussed and a solution is proposed to circumvent its difficulties. Quantum noise in gravitational interferometer has been extensively treated [5,12,13]. However, since the two arm Fabry–Perot cavities are antisymmetrically detuned, one would expect the effects related to the radiation pressure of the laser noise to be injected to the detection port as we shall discuss in the fifth section, and we show that a laser Relative Intensity Noise $RIN = 10^{-9}$ is needed to stick with the sensitivity curve of a non-detuned interferometer. We finally conclude in the last section. For the sake of simplicity, our calculations are based on the semiclassical theory [14]. In Advanced VIRGO, the plan is to fix the finesse of the long cavities around 400. The mirrors will weigh about 40 kg and be suspended with a meter-long wires. Arm cavities will be detuned by 10^{-3} to 10^{-2} nm. This detuning is to be compared with the cavity line-width 2.4 nm, and the wavelength $\lambda_0 \simeq 1064$ nm, i.e. $\omega_0 \simeq 1.77 \times 10^{15}$ rd/s. Finally, the laser power will be 130 W. We use these values in the following.

2. Light–mirrors intra-cavity coupling

2.1. Generation of sidebands by mirrors motion

In this section, we settle the calculation framework that we will use to describe the coupling between mirrors and the intra-cavity wave propagating within the cavity. We assume a single cavity where mirrors are moving according to Fig. 2. We consider one vibrational mode of angular frequency Ω. Motions of the mirrors are described according to:

$$x(t) = x_c \cos(\Omega t) + x_s \sin(\Omega t) \quad \text{and} \quad y(t) = y_c \cos(\Omega t) + y_s \sin(\Omega t)$$

Let us start by calculating the generation of sidebands by the mirrors motions. We use quite the same method described in Ref. [11] for the calculation of the sidebands generated by the gravitational wave. We consider the simple experiment in

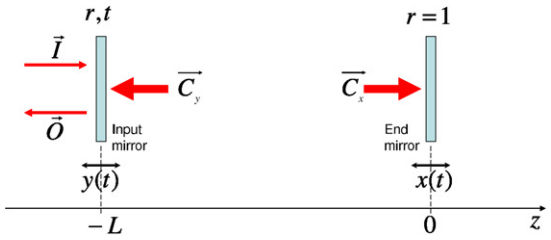

Fig. 2. Moving mirrors in arm cavities. x and y are small displacements compared to L. $\vec{I}$, $\vec{O}$, $\vec{C}_x$, $\vec{C}_y$ are electromagnetic waves.

which a classical photon is emitted from the input mirror at time t_0 at the position $z_l(t_0) = -L + y_c\cos(\Omega t_0) + y_s\sin(\Omega t_0)$, z_l represents the classical photon coordinate. We then obtain:

$$z_l(t) = c(t - t_0) - L + y_c\cos(\Omega t_0) + y_s\sin(\Omega t_0)$$

The light meets the cavity end mirror at the time t_1. Thus we have:

$$t_0 = t_1 - \frac{L}{c} + \frac{y_c}{c}\cos(\Omega t_0) + \frac{y_s}{c}\sin(\Omega t_0) - \frac{x_c}{c}\cos(\Omega t_1) - \frac{x_s}{c}\sin(\Omega t_1)$$

(x_c, x_s, y_c, y_s) represents small displacements compared to the cavity length L. Hence, at the order zero, we obtain $t_0 = t_1 - L/c$ and at the first order we get:

$$t_0 = t_1 - \frac{L}{c} + \frac{y_c}{c}\cos\left(\Omega t_1 - \frac{\Omega L}{c}\right) + \frac{y_s}{c}\sin\left(\Omega t_1 - \frac{\Omega L}{c}\right) - \frac{x_c}{c}\cos(\Omega t_1) - \frac{x_s}{c}\sin(\Omega t_1) \tag{1}$$

The last equation gives the time the light needs to cross the cavity once. We now consider a carrier wave with an angular frequency ω_0 surrounded by sidebands.[1] We also assume the sideband amplitude small compared to the carrier one. The scalar light wave amplitude is then expressed as:

$$A(t) = e^{-i\omega_0 t}\left(A_0 + \epsilon A_1 e^{-i\Omega t} + \epsilon A_2 e^{i\Omega t}\right)$$

where (A_0, A_1, A_2) are of the same order of magnitude, and $\epsilon \ll 1$. In the following we choose to write the light wave A for a given mode Ω as a 3 elements vector $\vec{A} = {}^t(A_0, A_1, A_2)$. We write down B as the wave obtained after propagation from the input mirror to the end mirror. We then have the relation $B(t_1) = A(t_0)$, which, to the first order, can be written using matrix notations $B = M_{12} \times A$. M_{12} is the propagation matrix which can be computed using Eq. (1) to give:

$$M_{12} = \begin{pmatrix} e^{i\Phi} & 0 & 0 \\ \frac{i}{2}(\chi - \eta e^{i\varphi})e^{i\Phi} & e^{i(\Phi+\varphi)} & 0 \\ \frac{i}{2}(\bar{\chi} - \bar{\eta} e^{-i\varphi})e^{i\Phi} & 0 & e^{i(\Phi-\varphi)} \end{pmatrix}$$

where $\Phi = \omega_0 L/c$, $\varphi = \Omega L/c$, $\chi(\Omega) = \frac{\omega_0}{\epsilon c}(x_c + i x_s) = \frac{2\omega_0}{\epsilon c}x(\Omega)$ and $\eta(\Omega) = \frac{\omega_0}{\epsilon c}(y_c + i y_s) = \frac{2\omega_0}{\epsilon c}y(\Omega)$. $x(\Omega)$ and $y(\Omega)$ represent the Fourier transforms of, respectively, $x(t)$ and $y(t)$. Similarly, we calculate the propagation matrix M_{21} from the end mirror to the input mirror:

$$M_{21} = \begin{pmatrix} e^{i\Phi} & 0 & 0 \\ \frac{i}{2}(\chi e^{i\varphi} - \eta)e^{i\Phi} & e^{i(\Phi+\varphi)} & 0 \\ \frac{i}{2}(\bar{\chi} e^{-i\varphi} - \bar{\eta})e^{i\Phi} & 0 & e^{i(\Phi-\varphi)} \end{pmatrix}$$

The round trip matrix is then $M_{121} = M_{21}M_{12}$. We have to take the motion of the input mirror into account while coupling waves between the extra-cavity and intra-cavity domains, i.e. to switch from a moving phase plane reference to a fixed one, and the other way around. This is described by the input and output matrices, namely M_i and M_o:

$$M_i = \begin{pmatrix} 1 & 0 & 0 \\ \frac{i}{2}\eta & 1 & 0 \\ \frac{i}{2}\bar{\eta} & 0 & 1 \end{pmatrix} \quad \text{and} \quad M_o = \begin{pmatrix} 1 & 0 & 0 \\ \frac{i}{2}\eta & 1 & 0 \\ \frac{i}{2}\bar{\eta} & 0 & 1 \end{pmatrix}$$

In the steady state regime, we have $\vec{C} = tM_i\vec{I} - rM_{121}\vec{C}$, which defines the cavity matrix $M_c = t(1 + rM_{121})^{-1}M_i$ by $\vec{C} = M_c\vec{I}$.

[1] In a first order calculation framework, the optomechanical coupling is linear. Therefore, the sidebands considered here are distant from the carrier by Ω.

The wave falling on the end mirror is $\vec{C_x} = M_{12}\vec{C} = M_{12}M_c\vec{I}$ and the wave falling on the input mirror is $\vec{C_y} = M_{121}\vec{C} = M_{121}M_c\vec{I}$. Therefore, we have:

- for the end mirror:

$$\begin{aligned}
C_{x0} &= e^{i\Phi}S(\omega_0)I_0\\
C_{x1} &= \frac{ie^{i\Phi}}{2t}S(\omega_0)S(\omega_0+\Omega)\big(\big[1-re^{2i(\Phi+\varphi)}\big]\chi + 2re^{i(2\Phi+\varphi)}\eta\big)I_0 + e^{i(\Phi+\varphi)}S(\omega_0+\Omega)I_1\\
C_{x2} &= \frac{ie^{i\Phi}}{2t}S(\omega_0)S(\omega_0-\Omega)\big(\big[1-re^{2i(\Phi-\varphi)}\big]\bar{\chi} + 2re^{i(2\Phi-\varphi)}\bar{\eta}\big)I_0 + e^{i(\Phi-\varphi)}S(\omega_0-\Omega)I_2
\end{aligned} \tag{2}$$

- for the input mirror:

$$\begin{aligned}
C_{y0} &= ie^{2i\Phi}S(\omega_0)I_0\\
C_{y1} &= -\frac{e^{2i\Phi}}{2t}S(\omega_0)S(\omega_0+\Omega)\big(2e^{i\varphi}\chi - \big[1-re^{2i(\Phi+\varphi)}\big]\eta\big)I_0 + ie^{2i(\Phi+\varphi)}S(\omega_0+\Omega)I_1\\
C_{y2} &= -\frac{e^{2i\Phi}}{2t}S(\omega_0)S(\omega_0-\Omega)\big(2e^{-i\varphi}\bar{\chi} - \big[1-re^{2i(\Phi-\varphi)}\big]\bar{\eta}\big)I_0 + ie^{2i(\Phi-\varphi)}S(\omega_0-\Omega)I_1
\end{aligned} \tag{3}$$

where $S(\omega) = t/(1+re^{i\omega L/c})$ is the cavity surtension factor [11]. The convention used above is to add a $\pi/2$ phase shift at each reflection, and no phase shift for the transmission [11]. In the same way, we calculate the reflected wave writing $\vec{O} = irM_oM_i\vec{I} + itM_oM_{121}M_C\vec{I} = iM_o(rM_i + tM_{121}M_c)\vec{I}$. It becomes:

$$\begin{aligned}
O_0 &= iR(\omega_0)I_0\\
O_1 &= -\big[\big(\chi + re^{i(2\Phi+\varphi)}\eta\big)S(\omega_0)S(\omega_0+\Omega)e^{i(2\Phi+\varphi)} + r\eta\big]I_0 + iR(\omega_0+\Omega)I_1\\
O_2 &= -\big[\big(\bar{\chi} + re^{i(2\Phi-\varphi)}\bar{\eta}\big)S(\omega_0)S(\omega_0-\Omega)e^{i(2\Phi-\varphi)} + r\bar{\eta}\big]I_0 + iR(\omega_0-\Omega)I_2
\end{aligned}$$

where $R(\omega) = (r+e^{2i\omega L/c})/(1+re^{2i\omega L/c})$ represents the cavity reflectivity [11].

2.2. Sideband radiation pressure on the cavity mirror

From now on, the magnitude $A(\omega,t)$ is defined as:

$$E_\omega(t) = \sqrt{\frac{\hbar\omega}{2\epsilon_0 c\sigma}}A_\omega(t)$$

where $E_\omega(t)$ is the complex notation of an electric field oscillating at the angular frequency ω and σ is the transverse section of the light beam (chosen constant for simplicity). This notation was used in Ref. [14] in such a way that $|A_\omega(t)|^2$ represents the classical numeric flow of photons. We consider the cavity mirror as a classical object and $x(t)$ its coordinate. Under the light wave $A_\omega(t)$ radiation pressure, we get:

$$M\frac{\mathrm{d}^2x}{\mathrm{d}t^2}(t) = -M\Omega_m^2x(t) - M\Gamma\frac{\mathrm{d}x}{\mathrm{d}t}(t) + \frac{2\hbar\omega_0}{c}\big|A(t)\big|^2 + F_m(\Omega) \tag{4}$$

where M is the mirror mass, $\Omega_m \simeq 2\pi \times 0.6$ Hz is the angular frequency of the pendulum, Γ is the damping constant, and F_m is the magnetic force used to control the mirror position for very low frequencies. Since the detection bandwidth is 10 Hz $< \Omega/2\pi <$ 10 kHz, we will consider F_m vanishing for $\Omega/2\pi \geqslant$ few hertz for the sake of simplicity. No Langevin force is considered since we assumed the detector limited by the quantum noise. In the frequency domain, Eq. (4) becomes for $\Omega \neq 0$:

$$x(\Omega) = X_m(\Omega)\left[F_m(\Omega) + \frac{2\hbar\omega_0}{c}(\epsilon\overline{A_0}A_1 + \epsilon A_0\overline{A_2})\right] \tag{5}$$

where we have used the usual definition of the mechanical susceptibility $X_m(\Omega) = [M(\Omega_m^2 - \Omega^2) - iM\Gamma\Omega]^{-1}$.

3. Optomechanical effects: the optical spring

When an optical cavity is resonant, a slight displacement of the mirrors does not change to the first order the intra-cavity power, and therefore the intra-cavity radiation pressure remains constant. Whereas for a non-resonant cavity, the same displacement makes the radiation pressure lower or higher which changes the dynamics of the mirror. Hence, the

radiation pressure acts like a force which depends on the mirror position, i.e. an optical spring [15]. To completely describe this phenomena, one has to take into account transients, and depending on the cavity detuning one can observe damping effects [16]. Although the detuning is very limited in Advanced VIRGO arm cavities, the intra-cavity power ($\simeq$1 MW) is very high and can enhance optical spring effects, likely to make mirror magnetic controls more difficult, or to change the sensitivity curve by changing the mirror dynamics in the detection frequency band.

3.1. Frequency dependent optical spring

Applying Eq. (5) to the cavity mirrors, we get:

- for the end mirror:

$$\chi = \frac{4\hbar\omega_0^2}{c^2} X_m(\Omega)(C_{x1}\overline{C_{x0}} + \overline{C_{x2}}C_{x0})$$

- for the input mirror:

$$\eta = -\frac{4\hbar\omega_0^2}{c^2} X_m(\Omega)(C_{y1}\overline{C_{y0}} + \overline{C_{y2}}C_{y0})$$

The sign $(-)$ explains that the radiation pressure is applied in the opposite direction. We then substitute Eqs. (2) and (3) into the last two formulas, which provides us with a set of two equations in χ and η:

$$\begin{aligned}\chi = -\eta = i\frac{4\omega_0}{c^2} X_m(\Omega) P_{cav}(\omega_0)\zeta_{\omega_0}(\Omega)[\chi - \eta] \\ + \frac{4\hbar\omega_0^2}{c^2} X_m(\Omega)\big[\overline{S(\omega_0)I_0}S(\omega_0+\Omega)I_1 + S(\omega_0)I_0\overline{S(\omega_0-\Omega)I_2}\big]\end{aligned} \tag{6}$$

$P_{cav}(\omega_0)$ designates the intra-cavity power. It appears then that the motion results from the wave introduced within the cavity and also from the sidebands generated by the motion itself. This remains true for any force acting on the mirror. The set of equations solved gives:

$$\chi = \frac{4\hbar\omega_0^2}{c^2} X_m(\Omega)\frac{\overline{S(\omega_0)I_0}S(\omega_0+\Omega)I_1 + S(\omega_0)I_0\overline{S(\omega_0-\Omega)I_2}}{1 - \frac{8i\omega_0}{c^2} X_m(\Omega) P_{cav}\zeta_{\omega_0}(\Omega)} \tag{7}$$

We have neglected the time delay between the two mirrors, which is usually called the quasi-static approximation [5], and we considered $r \simeq 1$. $\zeta_{\omega_0} = (e^{-2i\Phi}\overline{S(\omega_0-\Omega)} - e^{2i\Phi}S(\omega_0+\Omega))/t$ represents a symmetry function which vanishes when the cavity is resonant with ω_0, i.e. $2\Phi \equiv \pi[2\pi]$. Thus, at resonance, the radiation pressure motion results exclusively from the electromagnetic field fluctuations introduced to the cavity, whereas the effect of the generated sidebands $(+\Omega, -\Omega)$ interfere destructively. As we move away from the resonance, the symmetry between the sidebands is broken and the function ζ_{ω_0} increases.

We can also transform Eq. (7) to:

$$\chi = \frac{4\hbar\omega_0^2}{c^2}\frac{[\overline{S(\omega_0)I_0}S(\omega_0+\Omega)I_1 + S(\omega_0)I_0\overline{S(\omega_0-\Omega)I_2}]}{[k_m(\Omega) + k_{op}(\Omega)]} \tag{8}$$

where $k_{op}(\Omega)$ designates the optical spring which vanishes at resonance. $k_m(\Omega) = X_m(\Omega)^{-1}$ represents the frequency dependent mechanical spring. With some algebra, we get:

$$k_{op}(\Omega) = 2 \times \frac{8P_{cav}(\omega_0)}{x_p c}\frac{\delta\omega/\Omega_p}{(1 - i\frac{\Omega}{\Omega_p})^2}$$

where Ω_p is the angular frequency cavity pole and $x_p = L\Omega_p/\omega_0$ is the cavity half line-width. If δL is the cavity detuning in m, $\delta\omega = \omega_0\delta L/L$ is the angular frequency cavity detuning. The mirror dynamics are then governed by the sum $k_{eff}(\Omega) = k_m(\Omega) + k_{op}(\Omega)$. The optical spring is twice the usual one [16] because it is the sum of two identical optical springs, each one related to one moving mirror. These two optical springs are coupled in the quasi-static approximation. They might be anti-coupled at higher frequency. Nevertheless, as shown in Figs. 3a and 3b, for high frequency $k_{eff} \simeq k_m$ and optical spring effects become negligible.

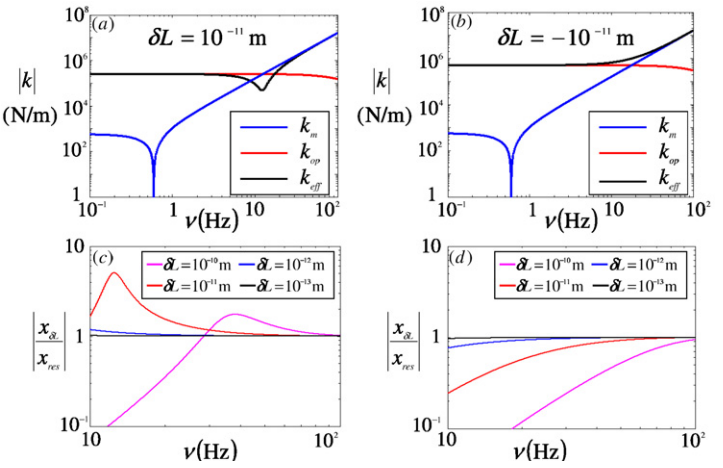

Fig. 3. (a) and (b): Behaviour of optical, mechanical and effective springs with the detuning. Depending on the sign of the detuning, the effective spring k_{eff} can be lower than the mechanical spring in a certain frequency band. The resonance quality factor is reduced whereas the resonance frequency gets close to the detection frequency band. (c) and (d): Radiation pressure displacements with respect to the resonance case. Increasing and decreasing radiation pressure effects by the modification of the system effective spring. The input power is 65 W.

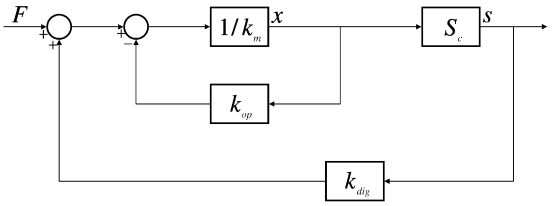

Fig. 4. Numerical mitigation of the optical spring. S is the cavity read-out function; F is a perturbation force, k_{dig} is the digital spring. A feedback filter, not shown, stabilises the system as if the optical spring was not present.

4. Mirror control issues

As shown in Fig. 3, for $\delta L \simeq 10^{-11}$ m the DC optical spring is about 1000 times higher than the suspension mechanical spring. Therefore, in one of the arms, the DC part of the spring will be negative for one of the two cavities. Thus the system is statically unstable. For higher frequencies, dynamical instabilities can also occur depending on the imaginary part of k_{eff}. This raises specific constraints on the mirror magnetic control. However, optical spring effects can be mitigated by adding, in parallel of the system, a digital spring as shown in Fig. 4. For all practical purposes, the locking of the interferometer will be acquired with a power where the effects of the optical spring are small enough to be negligible, then its power should be gradually increased.

5. Radiation pressure noise

Radiation pressure noise in gravitational wave antennae was first studied by C.M. Caves in 1980 [12,13] and designates the contribution of the quantum fluctuation of light to the detector sensitivity limitation. It is technically impossible to stabilise the power of a few tens of watts laser to its quantum level in the detection frequency band. However, as demonstrated by C.M. Caves, we shall show that for resonant cavities, the detector is purely sensitive to the vacuum fluctuations entering through the dark port. However, as shown in Fig. 3a, depending on the sign of the detuning, the spring k_{eff} can be lower than k_m in a limited frequency band, which shall enhance the mirror motion compared to the resonant case (Fig. 3c). Meanwhile, for the opposite detuning, the mirror motion is globally reduced (Figs. 3b and 3d). This effect contributes to increase the asymmetry between the two Michelson arms and thus contributes to inject the laser noise into the dark port. Related phenomenon such as optical cooling has already been studied and experimentally demonstrated so far in Refs. [16–18].

5.1. Non-power-recycled interferometer output

First, we consider the Fabry–Perot Michelson interferometer without power recycling. The Fabry–Perot cavities are adjusted out of resonance by an opposite amount $\delta L^n = -\delta L^w$ (superior (n) and (w) refer respectively to the north and west arms (Fig. 1)). At the bright port, we introduce an electromagnetic field described by the vector $\vec{\mathcal{A}}$, whereas at the dark port, the vacuum quantum fluctuation is introduced and described by the vector $\vec{\mathcal{V}}$.

In the following, we consider the beam splitter perfect and symmetric, which means $r_s = t_s = 1/\sqrt{2}$ and we stick with the same convention for reflection and transmission amplitudes. Since the sidebands are very small, we shall consider the two cavities identical except for the motion of the mirrors described respectively by χ^n and χ^w. In fact, as stated in the last section, the motion of mirrors due to radiation pressure depends on the cavity detuning. Therefore, except for χ, no superior will be used in the sidebands expressions. The dark port output vector $\vec{\Sigma}$ is:

$$\begin{aligned}
\Sigma_0 &= -\frac{1}{2}\big(R^n(\omega_0)e^{2i\Psi^n} + R^w(\omega_0)e^{2i\Psi^w}\big)\mathcal{A}_0 \\
\Sigma_1 &= iS(\omega_0)S(\omega_0+\Omega)\big[\chi^n e^{2i\Psi^n} + \chi^w e^{2i\Psi^w}\big]\mathcal{A}_0 - \frac{1}{2}R(\omega_0+\Omega)\big[\mathcal{A}_1\big(e^{2i\Psi^n} + e^{2i\Psi^w}\big) + i\mathcal{V}_1\big(e^{2i\Psi^n} - e^{2i\Psi^w}\big)\big] \\
\Sigma_2 &= iS(\omega_0)S(\omega_0-\Omega)\big[\bar{\chi}^n e^{2i\Psi^n} + \bar{\chi}^w e^{2i\Psi^w}\big]\mathcal{A}_0 - \frac{1}{2}R(\omega_0-\Omega)\big[\mathcal{A}_2\big(e^{2i\Psi^n} + e^{2i\Psi^w}\big) + i\mathcal{V}_2\big(e^{2i\Psi^n} - e^{2i\Psi^w}\big)\big] \qquad (9)
\end{aligned}$$

where $\Phi = (\Phi^n + \Phi^w)/2$, $S(\omega) = (S^n(\omega) + S^w(\omega))/2$ and $R(\omega) = (R^n(\omega) + R^w(\omega))/2$ which represent the order 0 of the development according to $\Delta\Phi = \omega_0\delta L/c \ll 1$ of respectively $\Phi^{n,w}$, $S^{n,w}$ and $R^{n,w}$. We have also $\Psi^{n,w} = l^{n,w}\omega_0/c$ and we neglected $\psi^{n,w} = l^{n,w}\Omega/c$. The order 0 of the optical spring k_{op} vanishes. Its first order is:

$$k_{op}^n(\Omega) = 16\frac{\omega_0}{c^2}P_{cav}\frac{F}{2\pi}S(\omega_0+\Omega)^2\Delta\Phi = k_{op}(\Omega)$$

and $k_{op}^w(\Omega) = -k_{op}(\Omega)$. We will consider the contribution of the first order development of $\Delta\Phi$ for the optical spring term (the denominator in Eq. (7)), because in the low frequency domain of the detection band, its absolute value is close to the mechanical spring. No Taylor series development can then be considered in the denominator of Eq. (8) right member. We define $\Psi = \Psi^n + \Psi^w$ and $\Delta\Psi = \Psi^n - \Psi^w$. We then obtain:

$$\Sigma_0 = -\big(\cos(\Delta\Psi)R(\omega_0) + i\sin(\Delta\Psi)\Delta R(\omega_0)\big)e^{i\Psi}\mathcal{A}_0$$

The Michelson is adjusted on the dark fringe, so we have $\cos(\Delta\Psi) = 0$ and $\sin(\Delta\Psi) = 1$. Hence, Eqs. (9) give:

$$\Sigma_1 = i\frac{\frac{8\hbar\omega_0^2 F}{\pi c^2}S(\omega_0+\Omega)^2 e^{i\Psi}}{k_m(\Omega)^2 - k_{op}(\Omega)^2}\big[-k_m(\Omega)(\bar{\mathcal{A}}_0\mathcal{V}_1 - \mathcal{A}_0\bar{\mathcal{V}}_2) + ik_{op}(\Omega)(\bar{\mathcal{A}}_0\mathcal{A}_1 + \mathcal{A}_0\bar{\mathcal{A}}_2)\big]\mathcal{A}_0 + e^{i(\Psi+\Phi+\varphi)}R(\omega_0)\mathcal{V}_1 \qquad (10)$$

and $\overline{\Sigma_2}(\Omega) = \overline{\Sigma_1}(-\Omega)$. The first term in the second member of Eq. (10) represents the radiation pressure noise whereas the second term represents the shot noise. When the cavity is resonant with the carrier, $k_{op} = 0$ which cancels the contribution of the laser fluctuations sidebands. The radiation pressure noise is therefore purely due to the vacuum fluctuations entering the interferometer through the dark port as was firstly stated by Caves in 1980 [12,13]. For $k_{op} \neq 0$, the laser fluctuations contribution does not vanish and we will see later that it can dominate the detector noise.

In the following, we become interested in the spectral density of noise of the power received on the photodiode at the interferometer dark port. In the time domain, the electromagnetic field received by the photodiode is $\Sigma(t) = \Sigma_0 + \delta\Sigma(t)$, whereas in the frequency domain, it is written $\Sigma(\Omega \neq 0) = \delta\Sigma(\Omega)$ where $\delta\Sigma(\Omega) = \epsilon\Sigma_1$, and consequently $\delta\Sigma(-\Omega) = \epsilon\Sigma_2$. In the same way, we shall define $\delta\mathcal{V}(\Omega) = \epsilon\mathcal{V}_1$, $\delta\mathcal{V}(-\Omega) = \epsilon\mathcal{V}_2$, $\delta\mathcal{A}(\Omega) = \epsilon\mathcal{A}_1$ and $\delta\mathcal{A}(-\Omega) = \epsilon\mathcal{A}_2$.[2] If $P(t) = P_0 + \delta P(t)$ designate the fluctuating power, the relation $P(t) = \hbar\omega_0|\Sigma(t)|^2$ gives:

$$\delta P(\Omega) = \big[\overline{\Sigma_0}\delta\Sigma(\Omega) + \Sigma_0\overline{\delta\Sigma}(-\Omega)\big]\hbar\omega_0 \qquad (11)$$

Since $\Delta R(\omega_0) \simeq -4i\mathcal{F}\Delta\Phi/\pi$, the last equation becomes:

$$\begin{aligned}
\delta P(\Omega) = &-\frac{64\hbar\mathcal{F}^2\omega_0^2\Delta\Phi}{\pi^2c^2}P_0S(\omega_0+\Omega)^2k_{op}(\Omega)\frac{(\overline{\mathcal{A}_0}\delta\mathcal{A}(\Omega) + \mathcal{A}_0\overline{\delta\mathcal{A}}(-\Omega))}{k_m(\Omega)^2 - k_{op}(\Omega)^2} \\
&- \left[i\frac{64\hbar\mathcal{F}^2\omega_0^2\Delta\Phi}{\pi^2c^2}\frac{P_0S(\omega_0+\Omega)^2k_m(\Omega)}{k_m(\Omega)^2 - k_{op}(\Omega)^2} + \frac{4\hbar\omega_0\mathcal{F}\Delta\Phi}{\pi}R(\omega_0)\right]\overline{\mathcal{A}_0}\delta\mathcal{V}(\Omega) \\
&+ \left[i\frac{64\hbar\mathcal{F}^2\omega_0^2\Delta\Phi}{\pi^2c^2}\frac{P_0S(\omega_0+\Omega)^2k_m(\Omega)}{k_m(\Omega)^2 - k_{op}(\Omega)^2} - \frac{4\hbar\omega_0\mathcal{F}\Delta\Phi}{\pi}R(\omega_0)\right]\mathcal{A}_0\delta\bar{\mathcal{V}}(-\Omega) \qquad (12)
\end{aligned}$$

where we used $e^{i\Phi} = i$ at resonance and we defined $P_0 = \hbar\omega_0|\mathcal{A}_0|^2$ as the power impinging on the beam splitter. To calculate the noise spectral density of the output power, we use the Wiener–Khintchine theorem which is given by $S_P = S_{\delta P\overline{\delta P}} = \langle\delta P(\Omega)\overline{\delta P(\Omega)}\rangle$. According to Ref. [14], $S_{\mathcal{V}} = S_{\delta\mathcal{V}\overline{\delta\mathcal{V}}} = 1/2$ and $S_{\delta\mathcal{V}\delta\mathcal{V}} = S_{\delta\mathcal{A}\delta\mathcal{A}} = S_{\overline{\delta\mathcal{V}}\,\overline{\delta\mathcal{V}}} = S_{\overline{\delta\mathcal{A}}\,\overline{\delta\mathcal{A}}} = 0$,

[2] We should recall that $\delta\mathcal{V}(\Omega)$ is a reduced notation of $\delta\mathcal{V}(\omega_0+\Omega)$. Hence, $\delta\mathcal{V}(\Omega)$ and $\delta\mathcal{V}(-\Omega)$ represent two independent modes of the electromagnetic field. We assume the same thing for $\delta\mathcal{A}(\Omega)$ which is generally verified for most of noise sources.

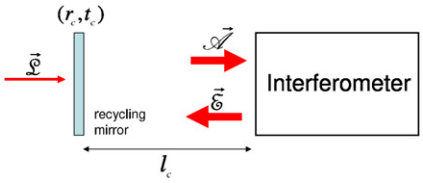

Fig. 5. Recycling system. The interferometer is considered as an input–output system.

$S_{\mathcal{A}} = S_{\delta_{\mathcal{A}}\delta_{\overline{\mathcal{A}}}} \neq 0$. Thus, it becomes:

$$S_P(\Omega) = \frac{P_0^2 P_{out}}{\hbar\omega_0}\left|\frac{16\hbar\mathcal{F}\omega_0^2}{\pi c^2}X_m(\Omega)\frac{S(\omega_0+\Omega)^2}{1-\frac{k_{op}^2}{k_m^2}}\right|^2\left[2\left|\frac{k_{op}}{k_m}\right|^2 S_{\mathcal{A}} + 1\right] + \hbar\omega_0 P_{out} \tag{13}$$

where $P_{out}(\Omega) = \hbar\omega_0|4\mathcal{F}\Delta\Phi/\pi|^2|\mathcal{A}_0|^2$ is the power received by the photodiode. We infer that for small detunings, the spectral density of noise is the quadratic sum of the radiation pressure noise and the shot noise as it is the case for resonant cavities [5]. Eq. (13) remains valid even when small asymmetries are taken into account, provided we have the right expression of P_{out}. In the following we calculate $S_{\mathcal{A}}$ in the case of a power-recycled interferometer.

5.2. Power-recycled interferometer

Power recycling was first proposed by R. Drever [19,20] and it aims at increasing the power impinging on the beam splitter. Also, as we will see in the following, it filters the laser power noise entering the interferometer, which, from now on, contributes to the limitation of the detector sensitivity.

In the following we will consider the interferometer as a single system (Fig. 5) the response of which is:

$$\begin{aligned}
\mathcal{E}_0 &= -iR(\omega_0)e^{i\Psi}\mathcal{A}_0\\
\mathcal{E}_1 &= \left[\frac{8\omega_0\mathcal{F}S(\omega_0+\Omega)^2k_mP_0}{\pi c^2(k_m^2-k_{op}^2)} + iR(\omega_0+\Omega)\right]e^{i\Psi}\mathcal{A}_1 + \frac{8\omega_0\mathcal{F}S(\omega_0+\Omega)^2k_mP_0}{\pi c^2(k_m^2-k_{op}^2)}e^{i\Psi}\bar{\mathcal{A}}_2\\
\bar{\mathcal{E}}_2 &= +\frac{8\omega_0\mathcal{F}S(\omega_0+\Omega)^2k_mP_0}{\pi c^2(k_m^2-k_{op}^2)}e^{-i\Psi}\mathcal{A}_1 + \left[\frac{8\omega_0\mathcal{F}S(\omega_0+\Omega)^2k_mP_0}{\pi c^2(k_m^2-k_{op}^2)} - iR(\omega_0+\Omega)\right]e^{-i\Psi}\bar{\mathcal{A}}_2
\end{aligned} \tag{14}$$

where we have neglected the contribution of the vacuum fluctuations and considered $\mathcal{A}_0$ real for the sake of simplicity.

5.2.1. Recycling the carrier

It is easy to demonstrate that in the steady state regime:

$$\mathcal{A}_0 = \frac{t_c e^{i\theta}}{1 + r_c e^{i(2\theta+\Psi)}}\mathcal{L}_0$$

where $\theta = \omega_0 l_c/c$.

When $2\theta + \Psi \equiv \pi[2\pi]$, the carrier is recycled and one gets $\mathcal{A}_0 = \sqrt{G_0}\mathcal{L}_0$ with $G_0 = t_c^2/(1-r_c)^2$ (which we call the carrier recycling regime in the following). Compared to the laser, the recycled power is then $P_0 = G_0 P_L$, where P_L designates the laser power. Thus G_0 represents the recycling gain. $G_0 \simeq 50$ increases the light power impinging on the beam splitter to a level (few kW) we cannot directly reach.

5.2.2. Recycling the sidebands

In order to describe the sideband dynamics, we define for each 3-element vector $\vec{A}$ a 2-element vector $\vec{A}' = {}^t(A_1, \bar{A}_2)$ which allows us to define the $(2,2)$ Michelson bright port response matrix M_b as $\vec{\mathcal{E}}' = M_b\vec{\mathcal{A}}'$ based on Eqs. (14). Therefore, it is obvious that, in the carrier recycling regime, the matrix $M_r = t_c(1 - r_c\,\mathrm{diag}(i,-i)M_b)^{-1}$ is the sideband recycling matrix, i.e. $\vec{\mathcal{A}}' = M_r\vec{\mathcal{L}}'$ and we have

$$M_r = -t_c \times \begin{pmatrix} \frac{e^{i\theta}\left[(1+r_cR) + \frac{8ir_c\omega_0\mathcal{F}S^2k_mG_0P_L}{k_m^2-k_0p^2}\right]}{(1+r_cR)^2} & \frac{e^{-i\theta}\,\frac{8ir_c\omega_0\mathcal{F}S^2k_mG_0P_L}{k_m^2-k_0p^2}}{(1+r_cR)^2} \\ -\frac{e^{i\theta}\,\frac{8ir_c\omega_0\mathcal{F}S^2k_mG_0P_L}{k_m^2-k_0p^2}}{(1+r_cR)^2} & \frac{e^{-i\theta}\left[(1+r_cR) - \frac{8ir_c\omega_0\mathcal{F}S^2k_mG_0P_L}{k_m^2-k_0p^2}\right]}{(1+r_cR)^2} \end{pmatrix}$$

Therefore, the spectral density $S_{\mathcal{A}}$ can be calculated and we obtain:

$$S_{\mathcal{A}} = |G(\Omega)|^2 S_{\mathcal{L}} = \left|\frac{t_c}{1 + r_cR(\omega_0+\Omega)}\right|^2 S_{\mathcal{L}} \tag{15}$$

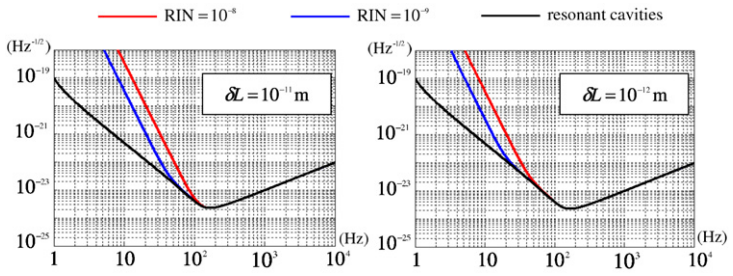

Fig. 6. Sensitivity curve for two detuning values.

We notice that the radiation pressure signal is not recycled, whereas the laser power noise is filtered by the recycling cavity. Usually, the laser noise is characterised by its *RIN* and we have:

$$S_{\mathcal{L}}(\Omega) = \frac{RIN(\Omega)^2}{2\hbar\omega_0/P_L}$$

5.3. Gravitational signal and sensitivity curve

According to Ref. [11], when $\varphi \ll 1$, a gravitational wave acts on the output signal like the motion of a mirror $x(\Omega) = Lh(\Omega)/2$. Sidebands generated by the gravitational wave act on the mirrors through radiation pressure. It is important to see that no forces are acting on the mirrors. Therefore, only the sideband contribution has to be taken into account in Eq. (6). The mirror motion resulting from the gravitational sidebands is:

$$\chi_{rad}(\Omega) = -\frac{1}{4}\frac{\omega_0 L}{\epsilon c}\left[\frac{k_{op}(\Omega)}{k_m(\Omega)+k_{op}(\Omega)}\right]h(\Omega) \quad \text{and} \quad \eta_{rad} = -\chi_{rad}$$

For the other cavity, both k_{op} and h change of sign for a $(+)$ polarisation gravitational wave. The Michelson is tuned on its dark fringe. The antisymmetric part of the radiation pressure gravitational signal is then:

$$\delta\Sigma_h^{rad} = -\frac{e^{i\Psi}}{2}\sqrt{\frac{2\mathcal{F}}{\pi}}S(\omega_0+\Omega)\left(\frac{\omega_0 L}{c}\right)\left[\frac{k_{op}(\Omega)^2}{k_m(\Omega)^2-k_{op}(\Omega)^2}\right]\sqrt{\frac{G_0 P_L}{\hbar\omega_0}}h(\Omega)$$

whereas the relativistic gravitational signal is:

$$\delta\Sigma_h^{rel} = -\frac{e^{i\Psi}}{2}\sqrt{\frac{2\mathcal{F}}{\pi}}S(\omega_0+\Omega)\left(\frac{\omega_0 L}{c}\right)\sqrt{\frac{G_0 P_L}{\hbar\omega_0}}h(\Omega)$$

We finally infer the spectral density of the gravitational signal as:

$$S_h(\Omega) = \frac{2\mathcal{F}}{\pi}\left(\frac{\omega_0 L}{c}\right)^2\left|S(\omega_0+\Omega)\right|^2 G_0 P_L P_{out}\left|\frac{k_m(\Omega)^2}{k_m(\Omega)^2-k_{op}(\Omega)^2}\right|^2\left|h(\Omega)\right|^2$$

The detector is characterised by its signal to noise ratio *SNR* defined by:

$$SNR = \sqrt{\frac{S_h(\Omega)}{S_P(\Omega)}}$$

We assumed, as stated above, that the detector is limited by the quantum noise. The sensitivity of the detector is defined as $|h(\Omega)|$ for $SNR = 1$. Hence, we have,

$$\left|h(\Omega)\right| = \left[\frac{128 G_0 P_L \hbar\mathcal{F}\omega_0}{\pi c^2 L^2}\left|S(\omega_0+\Omega)\right|^2\frac{[|k_m(\Omega)|^2+2|k_{op}(\Omega)|^2|G(\Omega)|^2 S_{\mathcal{L}}]}{|k_m(\Omega)|^4} + \frac{\pi\hbar c^2}{2G_0 P_L\mathcal{F}L^2\omega_0|S(\omega_0+\Omega)|^2}\left|1-\frac{k_{op}(\Omega)^2}{k_m(\Omega)^2}\right|^2\right]^{1/2}$$

The sensitivity curve is displayed in Fig. 6 for different detunings and laser *RIN* values. We notice that the radiation pressure noise dominates the sensitivity curve for low frequency and is mainly due to the laser power noise. It is, however, possible to reach the quantum limits as for resonant cavities, by reducing the *RIN* of the laser (10^{-9} seems to be a technical limit for now) and reducing the cavities detuning. Evidently, all noise sources are to be taken into account. For example, close to 10 Hz, the sensitivity should be limited by the seismic noise, whereas at 60 Hz, it should be limited by the mirrors

thermal noise. Nevertheless, compensating symmetry defects by detuning cavities seems to be a constraining procedure. Acting on the small Michelson, i.e. the Michelson without the Fabry–Perot cavities, might be a better solution because it keeps the cavity resonant and cancels all optical spring effects.

6. Conclusion

In this article, we have described some optomechanical issues in the future generation of the gravitational wave detector VIRGO. Arm cavities are planned to be detuned for the DC read-out detection schema implementation. However, we have shown that it should put some important constraints on the mirrors control system and also on the laser power stabilisation due to the dissymmetry between the Michelson arms. Moreover, the performance of the signal recycling technic needs to be revisited while taking into account the arms cavities detuning.

However, it is worth noting that our results do not match LIGO simulations. This issue is being investigated.

Acknowledgements

We would like to thank Dr. Alain Brillet and Dr. Pierre François Cohadon for stimulating discussions.

References

[1] A. Brillet, et al., VIRGO: Proposal for the construction of a large interferometric detector of gravitational waves, 1989, unpublished.
[2] M. Puntoro, The VIRGO sensitivity curve, VIRGO internal note VIR-NOT-PER-1390-51, 2004, and http://www.virgo.infn.it/senscurve.
[3] P. Amico, et al., Monolithic fused silica suspension for the VIRGO gravitational waves detector, Rev. Sci. Instrum. 73 (2002) 3318.
[4] B. Mours, E. Tournefier, J.-Y. Vinet, Thermal noise reduction in interferometric gravitational wave antennas using high order TEM modes, Class. Quantum Grav. 23 (2006) 5777.
[5] H.J. Kimble, Y. Levin, A.B. Matsko, K.S. Thorne, S.P. Vyatchanin, Conversion of conventional gravitational-wave interferometers into quantum nondemolition interferometers by modifying their input and/or output optics, Phys. Rev. D 65 (2002) 022002.
[6] F. Acernese, et al., VIRGO status, Class. Quantum Grav. 25 (2008) 184001.
[7] S. Hild, et al., DC-readout of a signal-recycled gravitational wave detector, Class. Quantum Grav. 26 (2009) 055012.
[8] A. Buonanno, Y. Chen, Quantum noise in second generation, signal-recycled laser interferometric gravitational-wave detectors, Phys. Rev. D 64 (2001) 042006.
[9] A. Buonanno, Y. Chen, Signal recycled laser-interferometer gravitational-wave detectors as optical springs, Phys. Rev. D 65 (2002) 042001.
[10] A. Buonanno, Y. Chen, N. Mavalvala, Quantum noise in laser-interferometer gravitational-wave detectors with a heterodyne readout scheme, Phys. Rev. D 67 (2003) 122005.
[11] J.Y. Vinet, The VIRGO physics book: Optics and related topics, http://www.cascina.virgo.infn.it/vpb/, 2006.
[12] C.M. Caves, Quantum-mechanical radiation-pressure fluctuations in an interferometer, Phys. Rev. Lett. 45 (1980) 75.
[13] C.M. Caves, Quantum-mechanical noise in an interferometer, Phys. Rev. D 23 (1981) 1693.
[14] C. Fabre, S. Reynaud, Quantum noise in optical systems: A semiclassical approach, in: J. Dalibard, J.M. Raimond, J. Zinn-Justin (Eds.), Session LIII, Les Houches, 1990.
[15] B.S. Sheard, M.B. Gray, C.M. Mow-Lowry, D.E. McClelland, Observation and characterization of an optical spring, Phys. Rev. A 69 (2004) 051801.
[16] O. Arcizet, P.-F. Cohadon, T. Briant, M. Pinard, A. Heidmann, Radiation-pressure cooling and optomechanical instability of a micromirror, Nature 444 (2006) 71.
[17] O. Arcizet, T. Briant, A. Heidmann, M. Pinard, Beating quantum limits in an optomechanical sensor by cavity detuning, Phys. Rev. A 73 (2006) 033819.
[18] C.M. Mow-Lowry, A.J. Mullavey, S. Goßler, M.B. Gray, D.E. McClelland, Cooling of a gram-scale cantilever flexure to 70 mK with a servo-modified optical spring, Phys. Rev. Lett. 100 (2008) 010801.
[19] R.W.P. Drever, in: N. Deruelle, T. Piran (Eds.), Gravitational Radiation, North-Holland, Amsterdam, 1983, p. 321.
[20] J.Y. Vinet, B. Meers, C.N. Man, A. Brillet, Optimization of long-baseline optical interferometers for gravitational-wave detection, Phys. Rev. D 38 (1988) 433.